arXiv:0801.1712v1 [physics.optics] 11 Jan 2008

Observation of Enhanced Beaming from Photonic Crystal Waveguides

Steven K. Morrison and Yuri S. Kivshar
Nonlinear Physics Centre and Centre for Ultrahigh-bandwidth Devices for Optical Systems (CUDOS), Australian National University, Canberra ACT 0200, Australia

We report on the experimental observation of the beaming effect in photonic crystals enhanced via surface modes. We experimentally map the spatial field distribution of energy emitted from a subwavelength photonic crystal waveguide into free-space, rendering with crisp clarity the diffractionless beaming of energy. Our experimental data agree well with our numerical studies of the beaming enhancement in photonic crystals with modulated surfaces. Without loss of generality, we study the beaming effect in a photonic crystal scaled to microwave frequencies and demonstrate the technological capacity to deliver long-range, wavelength-scaled beaming of energy.

PACS numbers: 42.70.Qs, 42.60.Jf, 42.25.Fx, 78.68.tm

Free-space propagation of light is inherently linked to diffraction; especially so when the beam emerges from a subwavelength aperture [1]. A consequence of tight confinement of electromagnetic waves is the large angular diffraction experienced by the waves abruptly released from the strong confinement. This substantial diffraction produced by subwavelength apertures is contradictory to the formation of a highly collimated beam. This contradiction can, however, be brought to accord and a narrow beam fashioned through the coherent coupling of additional slowly radiating surface waves on the portal surface surrounding the diminutive aperture. The radiating surface waves behave as Huygens-styled sources that combine and interfere constructively and destructively with all the emissions from the aperture to form a narrowly confined beam that exhibits diffraction free propagation over substantial distances [2].

Beaming of light from a subwavelength aperture was first experimentally demonstrated in metallic thin films flanked by periodic corrugations, with surface plasmons employed to transform the emissions into a confined beam of light [3]. Through insightful comparisons, beaming from subwavelength waveguides in photonic crystals was theoretically predicted [4] and independently observed in experiment [5]. Further research was conducted into the enhancement of the beaming effect from photonic crystal waveguides through the engineering of the modulated surfaces of photonic crystals [6, 7].

Important factors in the attainment of free-space beaming from photonic crystal waveguides are the efficient coupling from waveguide mode to the surface modes and the slow coupling and steering of radiated surface modes, such that their collective spatial phase and amplitudes superimpose and interfere destructively everywhere but directly in front of the waveguide aperture [4]. Monatomic photonic crystals support surface modes through an introduction of a defect structure to the surface layer. These surface modes occur below the light line (the free-space continuum of states) and decay evanescently away from the surface, and like the waveguide mode, occur within the photonic crystal's bandgap. If the surface defect structure of a photonic crystal is also periodically modulated or corrugated, these important factors required for beaming can be obtained [4, 6].

In this Letter we verify experimentally earlier theoretically predictions and demonstrate a substantially enhanced beaming of light from a photonic crystal waveguide of subwavelength width. We highlight the methods used to improve coupling between the photonic crystal waveguide mode and surface modes, and illustrate how this coupling is compatible with setting the correct phase delay and emission direction of the radiative surface modes to achieve highly collimated beaming. Furthermore, we demonstrate the substantial distance over which the beam remains diffractionless and reveal the Bessel-like beam profile supporting this extensive beaming range.

We commence our investigation into the beaming effect

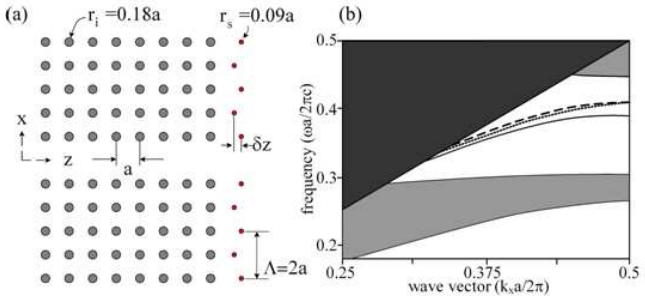


FIG. 1: (a) Square lattice, two-dimensional photonic crystal beaming model, illustrating the crystal's geometry, including a single-row defect waveguide and corrugated mono-defect surface layer in which surface cylinders have a radius of half the bulk photonic crystal's cylinder radius. (b) Dispersion relationship of the photonic crystal depicted in (a) along the direction of the surface where *even* number cylinders, numbered symmetrically and sequentially away from the waveguide are moved: (dashed line) towards the photonic crystal; (dotted line) positioned in line with odd number cylinders, removing the surface corrugation; and, (solid line) away from the photonic crystal. The dark upper triangle denotes the free-space continuum of states above the light line, whereas the other shaded regions depict the projected Bloch modes of the bulk photonic crystal.

by modeling an archetype photonic crystal using rigorous numerical methods. The model we employ is a photonic crystal with a square lattice populated with high dielectric cylinders, with dielectric constant of $\epsilon_r = 11.54$ (equal to the dielectric constant of alumina at $\sim 10GHz$, as used in the experiment confirmation) and of normalized radii $r = 0.18a$, where a is the lattice period. Photonic crystals of this configuration produce in-plane band-gaps in the normalized frequency band of $\omega = 0.3$ to $0.42 \times 2\pi c/a$ when the incident field is polarized with the electric field parallel to the axis of the cylinders. Through the removal of a single row of cylinders perpendicular to the surface, a single mode waveguide is created; whereas the defect surface structure used to induce a surface mode is composed of cylinders with a radius reduced by half. To co-join the surface modes and the directly transmitted field, a surface corrugation is formed by displacing alternative surface defect cylinders away from their lattice sites on the portal defect surface of the photonic crystal. The important geometric features of the photonic crystal model are illustrated in Fig. 1(a).

To reveal the critical properties of the photonic crystal model, we calculate the dispersion relationships of the quasi-periodic, corrugated surface structures using an *ab initio* finite-difference time-domain (FDTD) method. The method represents the fields in complex notation and varies the phase relationship $\exp(i\mathbf{kr})$ at the periodic boundaries and across the one-dimensional Brillouin zone. The width of the super-cell used is $2a$, such that it includes the double-periodicity of the surface corrugation. To remedy band folding that occurs due to the doubled super-cell width, sources are introduced into every unit cell of the super-cell with phase values determined by Bloch theorem. Using this method, we determine that a red shift occurs in the surface mode frequency for a positive displacement (away from the crystal) of the corrugation forming cylinders, and conversely, a minor blue frequency shift occurs for negatively displaced corrugation forming cylinders, as shown in Fig. 1(b).

Next, we study the important issue of coupling to the surface modes. Again, using the FDTD method we measure the power coupled into the surface mode, under steady state and numerically converged conditions, as we alter the position of the surface cylinders closer to the waveguide. Movement of these surface cylinders produces maximum coupling for a forward displacement (away from the crystal). This forward displacement creates both a cavity-like mode that captures a large quantity of the field, as well as delivering a strong re-scattering of the surface mode from the subsequent surface cylinders in a direction close to the waveguide aperture, enabling strong initial shaping of the transmitted beam.

To achieve optimal beaming we note the need to achieve both strong coupling to the surface modes along with directional control and phase alignment of the re-scattered surface modes. From the numerical analysis of the serial coupling to the surface modes, we implement a positive surface corrugation. From the dispersion analysis, we control the spatial phase positioning of the radiative surface modes by altering the corrugation displacement in accordance with the results given by Fig. 1(b). This corrugation displacement is, however, tempered and fine-tuned by the radius of the surface defect cylinders that, in concert with the corrugation displacement, also contribute to the scattering direction of the leaky surface mode, and *ipso facto*, the operational frequency and group velocities of the surface modes. Optimal displacement of the surface corrugation cylinders for this photonic crystal is $0.4a$ away from their lattice sites. Figure 2 demonstrates the strong contrast between (a) the simple terminated photonic crystal with full-size surface cylinders and (b) the optimal beaming, occurring at $\omega = 0.378 \times 2\pi c/a$, with half-diameter surface cylinders, alternatively displaced positively by $0.4a$, starting from the waveguide aperture and with a periodicity of $2a$. From these results, we determine that 82% of the transmitted field is conveyed into the narrow directed emission that in comparison to the un-altered surface yields a 258% increase in power within the area of the centrally directed beam.

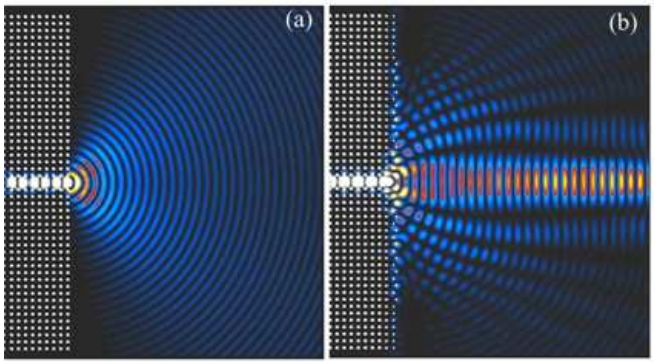


FIG. 2: Finite-difference time-domain simulations of the field intensity from the beaming modeling with (a) illustrating the full angle diffused output from the sub-wavelength waveguide exit when the surface structure is simply terminated in a row of cylinders equal in radius to those of the bulk photonic crystal, and (b) illustrating the highly collimated beam emitted from the waveguide having been strongly fashioned by radiative surface states.

Experimental fabrication of this photonic crystal for operation at optical wavelengths is very challenging, requiring significant fabrication resources. In order to confirm enhanced beaming, yet avoid these fabrication complexities, we scale the crystal to microwave wavelengths centered around 10GHz, where the lattice period is 11mm and use alumina cylinders with a refractive index of ~ 3.4. Figure 3 shows a schematic of the experimental setup with broadband source and detection facilitated by a 20GHz vector network analyzer (Rohde and Schwartz ZVB20) interfaced to half-wavelength dipole antennas. To achieve a low impedance transition from the unbalanced coaxial cable connected from the vector network

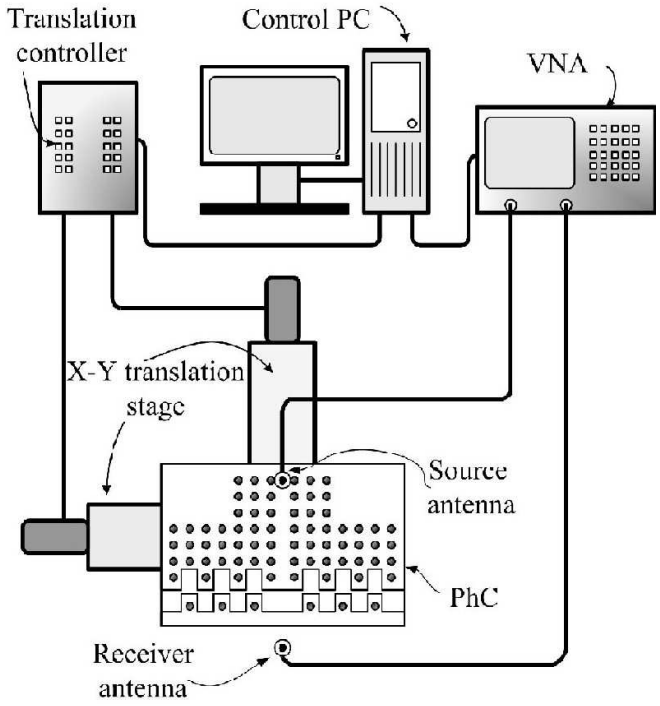


FIG. 3: Schematic representation of the pertinent elements and experimental configuration used to map the field intensity of the beaming effect.

analyzer (the conductors of the coax do not connect to the antenna in the same way and are thus unbalanced) to the symmetrical, balanced dipole antenna, a miniature sleeve balun with a 1 : 1 impedance transform was used. The source dipole antenna inserted into the crystal's waveguide excites a waveguide mode with an electric field parallel to both the antenna and cylinder axis after approximately four periods along the waveguide, as confirmed by FDTD simulations. Electromagnetic energy not coupled into the waveguide mode exits the rear of the waveguide. We mount the detector antenna to a tripod in front of the photonic crystal. Finally, to map the transmitted field, we mount the photonic crystals to an X-Y translation stage and use a phase maintaining cable between the source dipole antenna and the network analyzer, thus removing any phase noise occurring due to the disturbance of the cabling as the translation stage moves while mapping the transmitted field.

Figure 4 shows the surface structure of the crystal formed with 1mm radius cylinders with a corrugation period of $2a$. The surface corrugation displacement, Δz, is slide adjustable as illustrated in the inset of Fig. 4. This adjustable corrugation displacement allows adjustment and fine-tuning of the beaming effect to overcome experimental discrepancies in, for example, the dielectric constant of the alumina cylinders. We sample the field on a 5mm grid, equating to approximately 6 points per wavelength, and then interpolate the measured result using a two-dimensional cubic spline; Fig. 5 illustrates the results at 10.4GHz with a corrugation displacement of 4.44mm. Owing to impedance-mismatch return-losses between the 50Ω vector network analyzer, antennas and Bloch impedance of the photonic crystal's waveguide, the field is plotted in linear, normalized arbitrary units as indicated by the color scale.

Clearly shown in Fig. 5 is the crisp clarity of the mapped intensity field, revealing the long distance over which anomalously low divergence of the transmitted beam occurs, as well as demonstrating a strong correlation to the numerical result. Also clearly visible in Fig. 5 are the side lobes resulting from the grating effect of the surface corrugation, thus clearly confirming the theory that leaky surface modes shape the outgoing emission and transform the normally diffused output into an anomalously low diverging beam. Through mapping of the field without corrugation, we observer and affirm a strong, rapidly diffracting emission, absence of beaming. It is worth commenting that the long range diminishing of the experimental directed emission is to a large degree a result of the diffraction of the beam in the non-confined, out-of-plane direction resulting from the two-dimensional nature of the photonic crystal. Furthermore, the finite height of the experimental crystal (5λ) that is bounded by low dielectric constant Perspex plates causes spurious, destructive interference of the beam at approximately 20 wavelengths in front of the crystal's surface.

Cross-sectional slices of the normalized field intensity for both the numerical and experimental results are taken at a distance of $17\lambda_0$ in front of the portal surface of the photonic crystals and are presented in Fig. 6, with linear normalization taken with reference to the central intensity peak of the numerical results. Also clearly seen in Fig 6. is the Bessel-like beam profile, known to propagate

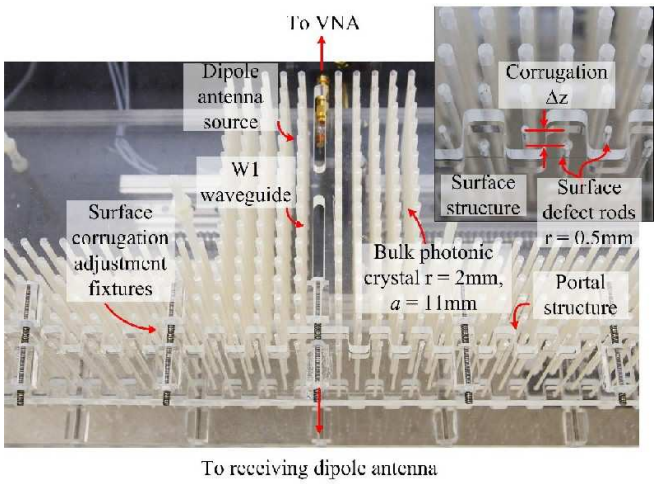


FIG. 4: Photograph of the experimental photonic crystal and portal surface. (Inset) Close-up of the photonic crystal's defect portal surface, highlighting the surface corrugation that, due to momentum conservation of the surface states, allows the surface modes to radiate into free space.

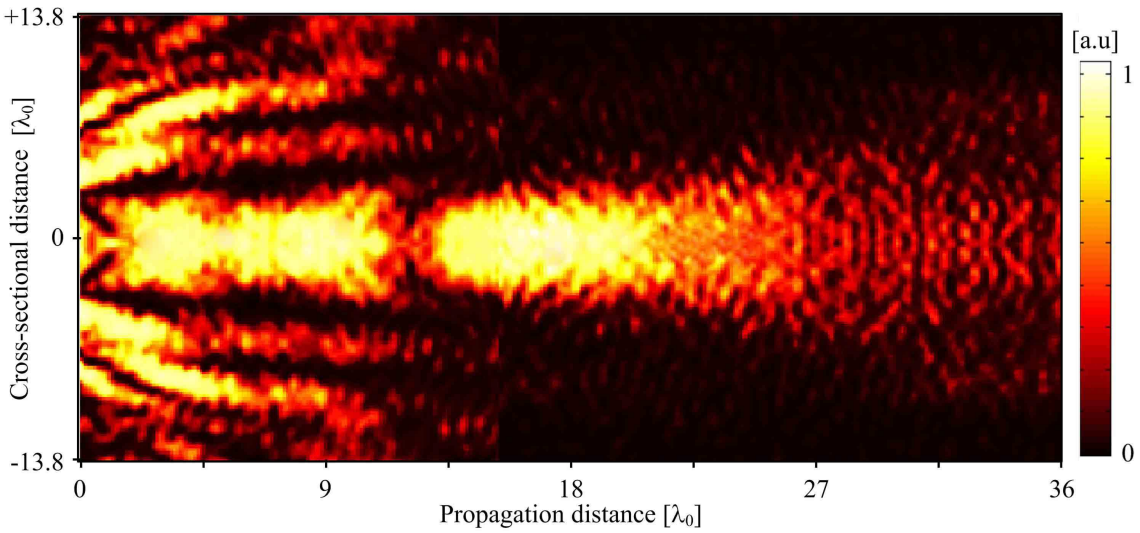


FIG. 5: Experimental map of the intensity field from the photonic crystal waveguide demonstrating the beaming effect at 10.4GHz in a plane central to the height of the crystal's cylinders and in front of the crystal's portal surface (spatial dimensions are given in free space wavelengths equivalent to 28.82mm).

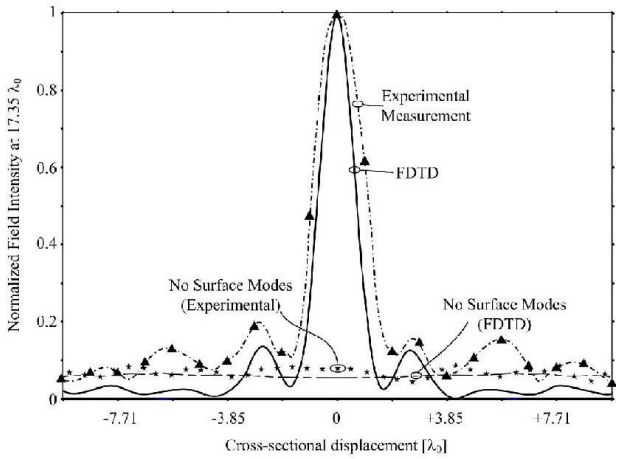


FIG. 6: Experimentally and numerically determined cross sections of the normalized field intensity at a distance of 17 λ_0 in front of the portal surface of the photonic crystal, demonstrating both virtually flat field distribution in the absence of radiating surface modes and highly collimated transmission, with Bessel-like profile, resulting from the beaming effect.

without diffraction over substantial distances, formed by the leaky surface modes.

In conclusion, we have studied, theoretically and experimentally, the conditions for dramatic enhancement of the free-space beaming of electromagnetic energy from a subwavelength photonic crystal waveguide. These conditions, that have a tendency to contend with each other, can be brought to accord such that optimal superposition of all emissions, both direct and re-scattered from the surface of the crystal, produce a highly collimated beam of wavelength dimensions. We have clearly demonstrated, with a strong correlation between our theoretical and experimental results, the role of the radiative surface modes in the fashioning of the directed emission with a Bessel-like beam profile capable of propagation over substantial distance without divergence. Our results hold great technological promise and perspectives for tailoring the beam profiles from subwavelength apertures in microwave, millimeter wave and optical systems.

This work has been supported by the Australian Research Council through the Discovery and Center of Excellence projects. We thank Dr. Ilya Shadrivov for useful discussions and help with experiments.

[1] H.A. Bethe, Phys. Rev. **66**, 163 (1944).
[2] D. Monroe, Phys. Rev. Focus. **13**, 11 (2004).
[3] T. W. Ebbesen, H. J. Lezec, H. F. Ghaemi, T. Thio, and P. A. Wolff, Nature **391**, 667 (1998).
[4] E. Moreno, F. J. Garcia-Vidal, and L. Martin-Moreno, Phys. Rev. B **69**, 121402(R) (2004).
[5] P. Kramper, M. Agio, C. M. Soukoulis, A. Birner, F. Muller, R. B. Wehrspohn, U. Gosele, and V. Sandoghdar, Phys. Rev. Lett. **92**, 113903 (2004).
[6] S. K. Morrison and Yu. S. Kivshar, Appl. Phys. Lett. **86**, 81110 (2005).
[7] S. K. Morrison and Yu. S. Kivshar, Appl. Phys. B **B81**, 343 (2005).